http://dx.doi.org/10.21577/0103-5053.20180206

J. Braz. Chem. Soc., Vol. 30, No. 3, 571-584, 2019
Printed in Brazil - ©2019 Sociedade Brasileira de Química

Article

Reduction Potential of Ru^{III}-Based Complexes with Potential Antitumor Activity and Thermodynamics of their Hydrolysis Reactions and Interactions with Possible Biological Targets: a Theoretical Investigation

Eufrásia S. Pereira,[a] Marcelo A. Chagas[a] and Willian R. Rocha *,[a]

[a]*Laboratório de Estudos Computacionais em Sistemas Moleculares (eCsMo[Lab]), Departamento de Química, Instituto de Ciências Exatas (ICEx), Universidade Federal de Minas Gerais, Pampulha, 31270-901 Belo Horizonte-MG, Brazil*

In this article density functional theory (DFT)-based calculations were employed to investigate the electrochemistry of the antitumor ruthenium complexes *trans*-tetrachloro(dimethylsulfoxide) imidazole ruthenate(III) (NAMI-A) and *trans*-[tetrachlorobis(1*H*-indazole)ruthenate(III)] (KP1019), their hydrolysis products as well as their interactions with biological S-donors and N-donors targets as cysteine, glutathione and guanine nucleobase. The compounds exhibit different electrochemical behavior upon hydrolysis. While the reduction potential of NAMI-A increases up to 0.8 V upon hydrolysis, the reduction potential of KP1019 remains almost constant after the first hydrolysis. NAMI-A and KP1019 complexes have thermodynamic preference to be reduced prior to undergoing hydrolysis and, strong preference to undergo successive hydrolysis instead of interacting with the S-donor and N-donor ligands. Interaction with S-donor ligands in the unprotonated form is highly unfavorable, with the free energy in solution (ΔG_{sol}) ≥ 18 kcal mol^{-1}. For both complexes, the interaction with the guanine and glutathione are of the same magnitude (ΔG_{sol} ca. –0.6 kcal mol^{-1}) meaning that these ligands can compete for binding to the metallodrug.

Keywords: density functional theory calculations, ruthenium-based metallodrugs, reduction potential, competitive biological reactions, solvent effects, electronic structure calculations

Introduction

Since the discovery of cisplatin and its use in the clinic therapy as one of the most effective anticancer drugs,[1,2] the research and development of metal-based drugs have received great attention from the scientific community.[3-5] Cancer is certainly among the leading causes of death in the world and, therefore, it has been the main target for the development of new drugs, especially those with antimetastatic activity. In spite of the great efficacy of platinum-based drugs against ovarian, bladder and testicular cancers, they display limited activity against some of the most common tumors, such as colon and breast cancers.[6-8] In addition, the high toxicity and incidence of drug resistance (acquired or intrinsic) remain the main challenges in their clinical application.[6] These facts stimulated the research of new metal-based drugs against cancer, aiming at improving clinical efficacy, reducing overall toxicity, and broadening the spectrum of activity.[4,5,9] In this regard, ruthenium complexes have been shown to be a very attractive platform, thanks to their low toxicity and low drug resistance. In addition, ruthenium has a range of oxidation states (Ru^{II}, Ru^{III} and Ru^{IV}) accessible under physiological conditions, which is unique among the platinum-group metals.[3,4] This is a very significant feature since the activities of most metal-based anticancer drugs are dependent on their oxidation states.

There are currently two antitumor compounds of ruthenium(III) (Figure 1) in the clinical phase, thanks to their broad antineoplastic activity: *trans*-[tetrachloro(dimethylsulfoxide)imidazole ruthenate(III)] ([Im]*trans*-[$RuCl_4$(Im)(DMSO)]), also known as NAMI-A,[10] and *trans*-[tetrachlorobis(1*H*-indazole)ruthenate(III)] ([IndH]*trans*-[$RuCl_4(Ind)_2$]), known as KP1019.[11] NAMI-A is able to effectively inhibit the development and growth of lung metastasis in experimental models of solid tumors *in vivo*,[12,13] whereas KP1019 shows cytotoxic activity by inducing apoptosis in a large line of cancer cells, especially colorectal tumors.[11,14,15]

*e-mail: wrocha@ufmg.br

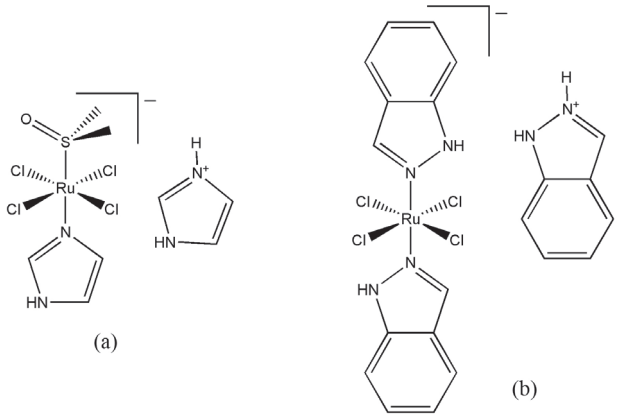

Figure 1. Structures of (a) NAMI-A and (b) KP1019.

Both complexes were considered as promising antitumor agents. However, NAMI-A is no longer in clinical trials due to side effects and antitumor activity less than expected,[16] whereas the indazolium counter ion in KP1019 has been replaced by the sodium (KP-1339/IT139) ion in order to increase the solubility and was selected for further development.[17] These results evidenced the need to know the individual chemical characteristics of the different ruthenium-based compounds for therapeutic purposes. Although both complexes underwent clinical trials phase, their mechanism of action is not yet fully understood. It is well known that Ru^{III} compounds are more inert toward ligand-exchange reactions than Ru^{II}.[3] Therefore, metallodrugs based on Ru^{III} need to be activated by reduction, which will accelerate the hydrolysis reactions and interactions with biological targets as was first proposed by Clarke.[3] Consequently, Ru^{III}-based drugs must have accessible reduction potentials in the biological medium. Electrochemical and chemical reduction studies of Ru^{III} metallodrugs are, therefore, of great importance in order to understand their biological activities and thus have been the subject of several studies.[18-27] Ravera *et al.*[25] investigated the redox chemistry of [LH][*trans*-$Ru^{III}Cl_4L_2$] (L = imidazole or indazole) complexes in water at different pH values. For the indazole and imidazole complexes the $E^{0'}$ (Ru^{III}/Ru^{II}) reduction potential of –0.160 and –0.460 V *vs.* Ag/AgCl was obtained at pH 4.0. The authors showed that despite the structural similarities, the electrochemically generated Ru^{II} species undergoes different ligand displacement reactions. Using nuclear magnetic resonance (NMR) experiments, the authors have also shown that one of the axial imidazole ligands is displaced by water in the imidazole complex $[Ru^{II}Cl_4(Im)_2]^{2-}$ and a Cl^-/water substitution takes place in the indazole complex $[Ru^{II}Cl_4(Ind)_2]^{2-}$. The chemical reduction in the presence of glutathione (GSH) was also observed by the authors. Reisner *et al.*[23] investigated the electrochemical behavior of [*trans*-$Ru^{III}Cl_4L(DMSO)$] and [*trans*-$Ru^{III}Cl_4L_2$] complexes (L = imidazole, 1,2,4-triazole, indazole) in dimethylformamide (DMF) and DMSO. For the NAMI-A and KP1019 complexes, $E^{0'}$ (Ru^{III}/Ru^{II}) reduction potentials of –0.220 and –0.720 V *vs.* normal hydrogen electrode (NHE) was found, respectively, in DMF. The authors showed that the general equation proposed by Lever,[28] which assumes an additive contribution of all the ligands to the redox potential of the complex, predicts very well the measured reduction potential of the Ru^{III} complexes, and they were able to propose an equation to predict the reduction potential of single negatively charged complexes of Ru^{III} in aqueous medium at pH 7. For the Na[$Ru^{III}Cl_4(DMSO)(Im)$] complex, Alessio *et al.*[19] obtained $E^{0'}$ (Ru^{III}/Ru^{II}) reduction potentials of –0.001 V *vs.* saturated sodium chloride calomel electrode (SSCE). The aquation reaction revealed to be pH dependent. In the pH range of 7.1 to 9.0 the final aquated product was $[Ru^{II}Cl_3(DMSO)(H_2O)(Im)]^-$ and, at pH 6 the final detected product was $[Ru^{II}Cl_4(DMSO)(H_2O)]^-$, with exchange of the imidazole ligand by water. It has been shown that at physiological pH and 37 °C (phosphate buffer, 0.9% NaCl), stepwise dissociation of two chloride ions from NAMI-A occurs within minutes.[29]

These Ru^{III} anticancer complexes have also been shown to be reduced by common biological reductants such as GSH and ascorbic acid. Hartmann *et al.*[20] showed that, at pH 7 and 0.1 M phosphate buffer, $(H_2Im)[RuCl_4(HIm)_2]$ is promptly reduced by GSH. Schluga *et al.*[24] showed that the binding of KP1019 toward the deoxyribonucleic acid (DNA)-modeling nucleotide guanosine monophosphate (GMP) is increased upon addition of GSH but not of ascorbic acid. That is, GSH reduces the Ru^{III} complex and facilitates the binding to the nucleotide. However, the mechanism involved in the chemical reduction of these Ru^{III} anticancer complexes is not yet fully understood. It is believed that an inner-sphere mechanism is involved.[21,30]

All these results suggest that in the mechanism associated with these Ru^{III} anticancer complexes, activation by reduction and exchange of chloride ligands by water molecules of the solvent (hydrolysis or aquation) are two important steps for the antitumor function of such metallodrugs. After being activated, distributed and located in cell compartments, the way the ruthenium metallodrugs kills the cancer cells is not well fully understood. In contrast with cisplatin which is well-known to interact with DNA, the primary interaction target(s) for the ruthenium metallodrugs is still an open question.

Based on the observations listed above, three events are connected with the biological activity of NAMI-A and KP1019: (*i*) reduction of the Ru^{III} center; (*ii*) chloride

exchange reaction with water molecules of the solvent medium; and (*iii*) interaction with the biological targets. These reactions can compete with each other, as schematically shown in Figure 2, for the NAMI-A compound. The compound can initially be reduced following pathway b, generating Ru^{II} complex **1b**, and this reduced complex can then undergo ligand exchange reaction with water of the solvent, generating the monoaquo complex **2**. Alternatively, the complex can initially undergo ligand displacement reaction, following pathway a, generating the monoaquo-Ru^{III} species **1a**, which is posteriorly reduced to the monoaquo-Ru^{II} species **2**. Once the reduced monoaquo-Ru^{II} species is formed other competitive processes can take place, as for instance the successive displacement of chloride by water through pathway c or direct interaction with the biological target **L**, pathway d, generating the adduct **3** in which the target **L** displaces a water molecule. The sequence of the events or, the preferred pathways, will depend on the kinetics of these reactions and also on the reduction potential of the species, chloride concentration and thermodynamic stability of the complexes formed.

There are some open questions related to the interaction of NAMI-A and KP1019 complexes with their final biological target, the last step shown in Figure 2. Some studies have suggested that NAMI-A acts on cell cycle blockade at the G2/M transition point, due to the accumulation of inactive Cdk1 proteins, which is responsible for reporting DNA molecule damage.[31,32] In addition, NAMI-A also causes inhibition of topoisomerase proteins, which are important enzymes in DNA replication and packaging processes.[33] On the other hand, it is believed that the cytotoxic activity of KP1019 is based on the endoplasmic reticulum (ER), with stress-related effects rather than DNA damage.[17] KP1019 has been shown to cause oxidative stress and perturbation of ER functions in cancer cells. In addition, the 78 kDa glucose regulatory protein (GRP78) is reduced to a normal level.[34,35] Thus, apoptosis is induced by intrinsic mitochondrial pathway.[36,37]

Therefore, despite the progress in the biochemical understanding of the biological activity of NAMI-A and KP1019, fundamental studies on the kinetic and thermodynamics of the competitive processes exemplified in Figure 2 can provide important information on the

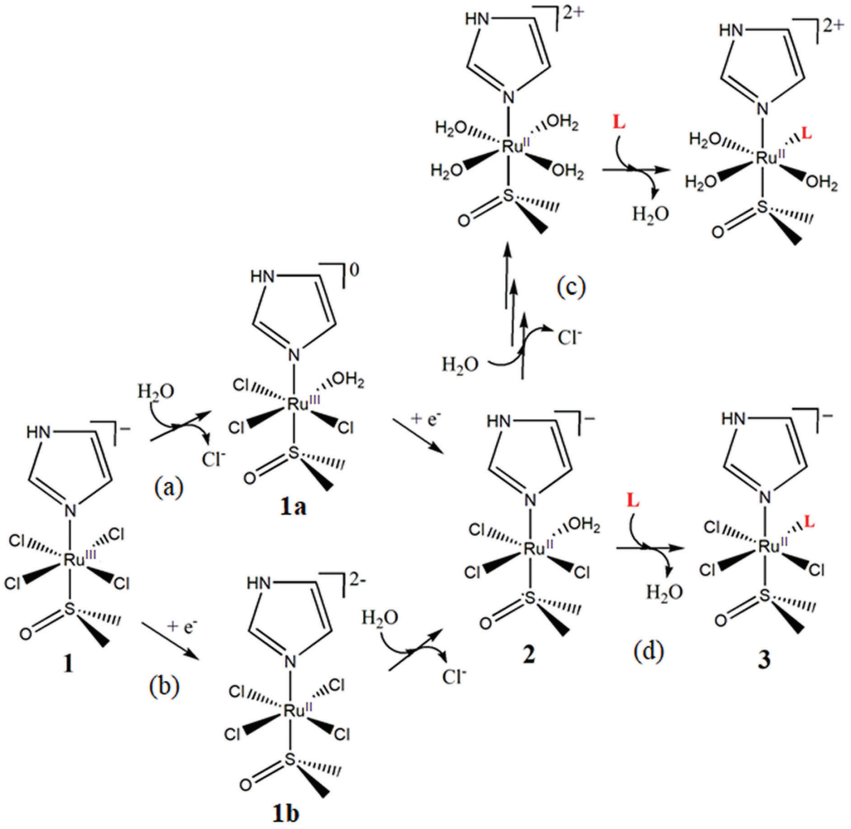

Figure 2. Schematic representation of the possible competitive biological reaction paths for the NAMI-A complex (**1**). In pathway (a) NAMI-A initially undergoes ligand displacement reaction generating the monoaquo-Ru^{III} species **1a**, which is posteriorly reduced to the monoaquo-Ru^{II} species **2**. In pathway (b) the compound is initially reduced generating Ru^{II} complex **1b** and undergoes ligand exchange reaction with water, generating the monoaquo complex **2**. After complex **2** is generated it can be consecutively hydrolyzed through pathway (c) or interact with the biological targets **L** in pathway (d), generating the adduct **3**.

bioavailability and reactivity of these compounds. In this regard, in the present work, we employed the density functional theory (DFT) to investigate the electrochemistry of NAMI-A, KP1019 and their hydrolysis products, as well as their interactions with S-donor targets cysteine (Cys) and GSH, and N-donor target guanine nucleobase (at the coordination sites N3 (GN3) and N7 (GN7)). We believe that the study of the different structural characteristics, as well as the thermodynamic properties of Ru^{II} adducts formation with some strategic biological targets and DNA nucleobases in solution, can provide important information to understand the interaction of these compounds in the cellular environment.

Methodology

Full unconstrained geometry optimizations and frequency calculations of all species involved in this work were carried out at the DFT level of theory[38] with the Tao, Perdew, Staroverov, and Scuseria hybrid meta-generalized gradient approximation (TPSSh) exchange-correlation functional[39] as implemented in the ORCA program.[40] The Ahlrichs full electron def2-triple-zeta valence polarization (TZVP) basis set[41] was used for all atoms. Scalar relativistic effects were treated using the zeroth order regular approximation (ZORA) formalism.[42-44] To speed up the calculations the resolution of the identity[45] was used for the Coulomb part and the chain of sphere approach[46] for the exchange part of the Fock matrix employing the def2-TZVP/J auxiliary basis set.[47] We have shown that this combination of exchange-correlation functional and basis set provides good structural and energetic results for a series of transition metal complexes[48] and also to describe the electronic spectrum of ruthenium-amine compounds.[49] Calculations on the open-shell structures were carried out within the unrestricted Kohn-Sham formalism. For the Ru^{III} species with d^5 configuration, only the S = 1 / 2 configuration was evaluated since it is the most stable spin state of Ru^{III} complexes.[50-52] The optimized Cartesian coordinates of all species studied in this work can be found in the Supplementary Information (SI) section.

The reduction potential of the complexes was calculated using equation 1, as shown by Rulíšek.[53]

$$E^0\,[V] = 27.21(G_{ox}\,[a.u.] - G_{red}\,[a.u.]) - E^0_{abs}(NHE)\,[V] \quad (1)$$

where G_{ox} and G_{red} are the Gibbs free energies of the oxidized and reduced forms, respectively. E^0_{abs} (NHE) is the absolute potential of the normal hydrogen electrode of 4.218 V, recommended by Isse and Gennaro.[54] Gibbs free energy of the species was obtained using equation 2:

$$G = E_{elec-nuc} + \Delta G_{solv} + G_{therm} \quad (2)$$

where ΔG_{solv} is the free energy of solvation, G_{therm} is the thermal contribution, obtained under the harmonic oscillator and rigid rotor approach and $E_{elec-nuc}$ is the total electronic and nuclear energy of the species. The ΔG_{solv} was obtained using the solvation model based on density (SMD) of Truhlar and co-workers[55] as implemented in the ORCA program,[40,55] in which the electrostatic contribution is obtained using the conductor-like screening model (COSMO) of Klamt and Schuurmann.[56] We have shown that this combination of methods/basis set provides good reduction potentials for ruthenium complexes.[52]

The Gibbs free energy for the interactions involving the Ru^{II}-monoaquo species and the biomolecules (GN3 and GN7 sites, Cys and GSH) were computed using the thermodynamic cycle exemplified in Figure 3 (for the KP1019 monohydrated compound), at the TPSSh/def2-TZVP level of theory.

Solvation free energies were computed as described before and the thermal corrections for the zero point energy at 298.15 K were obtained through harmonic frequency calculations at the TPSSh/def2-TZVP. The overall free energy in solution (ΔG_{sol}) was then computed using equation 3:

$$\Delta G_{sol} = \Delta G_g + \Delta(\Delta G_{solv}) \quad (3)$$

where ΔG_g is the free energy in gas phase and $\Delta(\Delta G_{solv})$

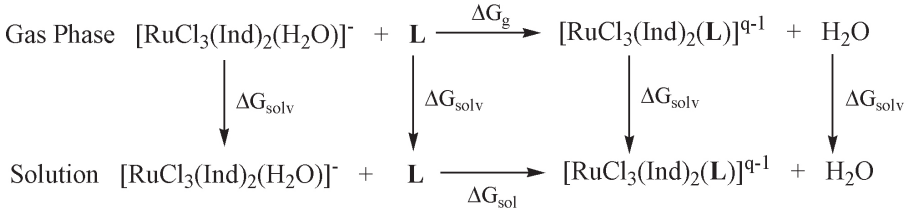

Figure 3. Example of the thermodynamic cycle used to compute the Gibbs free energy for the interaction of the Ru^{II}-monoaquo complexes with the biological molecules **L** (GN3 and GN7 sites, Cys and GSH). ΔG_g, ΔG_{solv} and ΔG_{sol} are the Gibbs free energy of the reaction in gas phase, of solvation and of the reaction in solution, respectively. q is zero when **L** is the protonated form of cysteine and glutathione (CysH, GSH) and the DNA nucleobases, and –1 when **L** is the anionic form of cysteine and glutathione (Cys^-, GS^-). When the protonated forms of Cys and GSH are used, the final products for these interactions contain H_3O^+ instead of H_2O.

is the difference in free energy of solvation of the species involved. All calculations were performed using the ORCA program package.[40]

Results and Discussion

Molecular structure, reduction potentials and hydrolysis reactions

The TPSSh/def2-TZVP optimized structures of NAMI-A and KP1019 are shown in Figure 4. The complexes show octahedral geometry around the metallic center and the computed structural parameters are in excellent agreement with the experimental findings[19,57] with deviations in the order of 0.01 Å in the bond lengths and 0.01° in the bond angles.

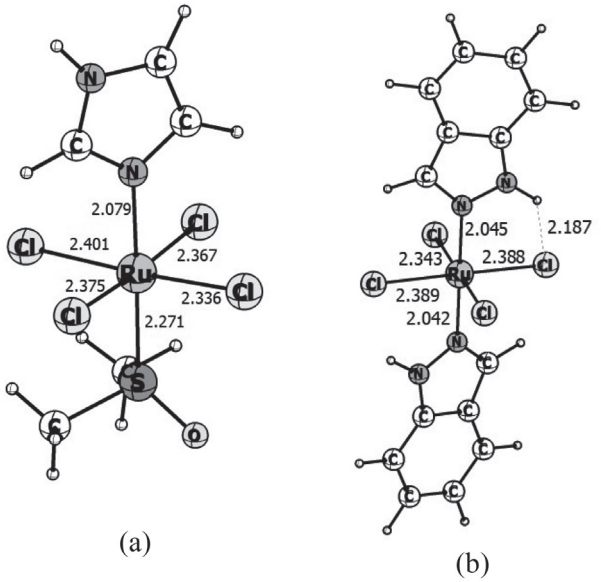

Figure 4. TPSSh/def2-TZVP optimized structures of (a) NAMI-A and (b) KP1019. Bond distances are given in Å.

It is worth noting that the KP1019 structure is stabilized by intramolecular hydrogen bonds of NH···Cl type, in accordance with the determined X-ray crystal structure.[23] When a rotation of 45° around the Ru-indazole bond is performed, the new generated structure is ca. 10 kcal mol^{-1} higher in energy. Therefore, the intramolecular hydrogen bonds have an important effect of stabilizing the KP1019 structure around 10 kcal mol^{-1}. Both NAMI-A and KP1019 are paramagnetic species and the calculations showed that the excess α spin densities is localized almost exclusively at the dz^2 orbital of the ruthenium center with $\rho_\alpha = 0.900$ for NAMI-A and $\rho_\alpha = 0.852$ for KP1019.

The calculated one electron reduction potentials of the NAMI-A, KP1019 and their respective products from the chloride ligand exchange with water are summarized in Table 1. As it can be seen, while the reduction potential of the KP1019 complex is unresponsive relative to chloride exchange, the reduction potential of NAMI-A increases 0.132 V after the first hydrolysis, and 0.361 and 0.443 V after the second hydrolysis in *cis* and *trans* positions, respectively. After the third hydrolysis, the reduction potential increases 0.795 V.

Table 1. Computed reduction potential for the NAMI-A, KP1019 and their hydrolysis products

n	Reduction potential *vs.* NHE / V	
	$[Ru(Cl)_{4-n}(H_2O)_n(Im)(DMSO)]^{-1+n}$	$[Ru(Cl)_{4-n}(H_2O)_n(Ind)_2]^{-1+n}$
0	0.0244 (0.235)[a]	0.289 (0.00-0.03)[b]
1	0.156	0.166
2	0.385 [0.467][c]	0.183 [0.176][c]
3	0.819	0.293

[a]Experimental value taken from reference 19; [b]experimental value taken from reference 23; [c]values in brackets are for the *trans* isomer. NHE: normal hydrogen electrode; n: number of water molecules involved in the exchange reaction with the chloride ligands; Im: imidazole; DMSO: dimethylsulfoxide; Ind: indazole.

Electrochemical studies conducted by Brindell *et al.*[58] have shown that the hydrolysis products of NAMI-A have redox potentials in the range of 0.187-0.597 V *vs.* NHE. The wave recorded at $E^0 = 0.597$ V was assigned to a mixture of $[RuCl_3(H_2O)(DMSO)(Im)]$ and $[RuCl_2(H_2O)_2(DMSO)(Im)]^+$, corresponding to an increase of 0.299 V when compared with the value of $E^0 = 0.298$ V measured for NAMI-A. An increase of the 0.12 V in the reduction potential of the monoaquo complex was also observed.[22,23] For the KP1019 complex, it is also observed an increase in the reduction potential after the first hydrolysis. Ravera *et al.*[25] measured the reduction potential of $[Ru^{III}(H_2O)Cl_3(Ind)_2]$ at –0.072 V *vs.* Ag/AgCl, which corresponds to an increase of 0.088 V compared with the KP1019 reduction potential. Therefore, the trend observed in our computed values for NAMI-A and its hydrolysis products are in line with the experimental findings and shows that it is easier to reduce the hydrolyzed products than the original compound. However, for the KP1019, our results show that the reduction potential decreases after the first hydrolysis, increases very little in the second hydrolysis and returns almost to its original value after the third hydrolysis. Therefore, the complexes show distinct electrochemical behavior, which may partially explain their biological diversity.

For both complexes, the lowest unoccupied molecular orbitals (LUMO), which can be directly correlated with the electron accepting capability of the complex, are located at the metallic center, as can be seen in Figures S1 and

S2 (SI section). The next orbitals LUMO + 1 are within 0.2-1.0 eV higher in energy and, therefore, the reduction process takes place effectively at the metallic center. In the KP1019 complex there is an indazole σ-donor ligand that contributes to increase the electronic density at the metallic center, making it more difficult to reduce. For the NAMI-A the π-acceptor DMSO ligand withdraws electron density from the metal, stabilizes the Ru^{II} species and facilitates the reduction. The increase of the reduction potential with subsequent hydrolysis is in qualitative agreement with the experimental results, showing an increase of the reduction potential for each chloride exchanged by water.[58,59]

Our TPSSh/def2-TZVP/SMD computed reduction potentials are in good agreement with the available experimental values. The variation observed may be related to description of the solvent effects as well as spin-orbit effects, as was pointed out by other authors for the reduction potential of some ruthenium-containing compounds.[60,61] In some cases, quantitative agreement is obtained only when explicit solvent molecules are employed. However, we have recently shown that the procedure used in this work produces excellent results for the reduction potential of ruthenium complexes with amine ligands.[52]

The TPSSh/def2-TZVP optimized structures for the products of the hydrolysis reactions of NAMI-A, in the +3 and +2 oxidation states, are shown in Figures 5 and 6, respectively, which highlight the main structural parameters around the metallic center. The optimized structures for the products of the hydrolysis reactions of KP1019, in the +3 and +2 oxidation states, are shown in Figures S3 and S4 (SI section), respectively. The thermodynamics associated with the chloride exchange reaction by water

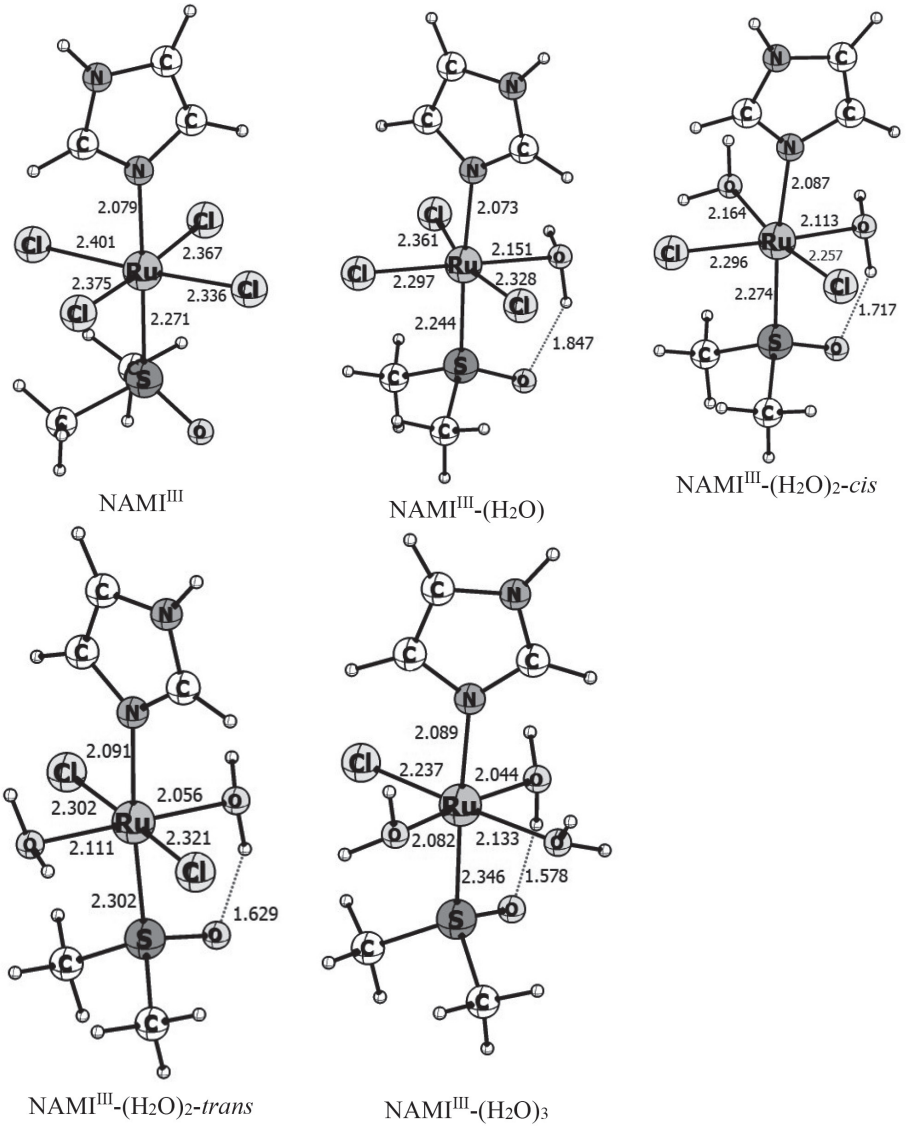

Figure 5. TPSSh/def2-TZVP optimized structures for the NAMI-A complex in the +3 formal oxidation state (NAMI^{III}) and its mono- (NAMI^{III}-(H_2O)), di- (NAMI^{III}-(H_2O)$_2$-*cis*, NAMI^{III}-(H_2O)$_2$-*trans*) and tri- (NAMI^{III}-(H_2O)$_3$) water substituted derivatives. Bond distances are given in Å.

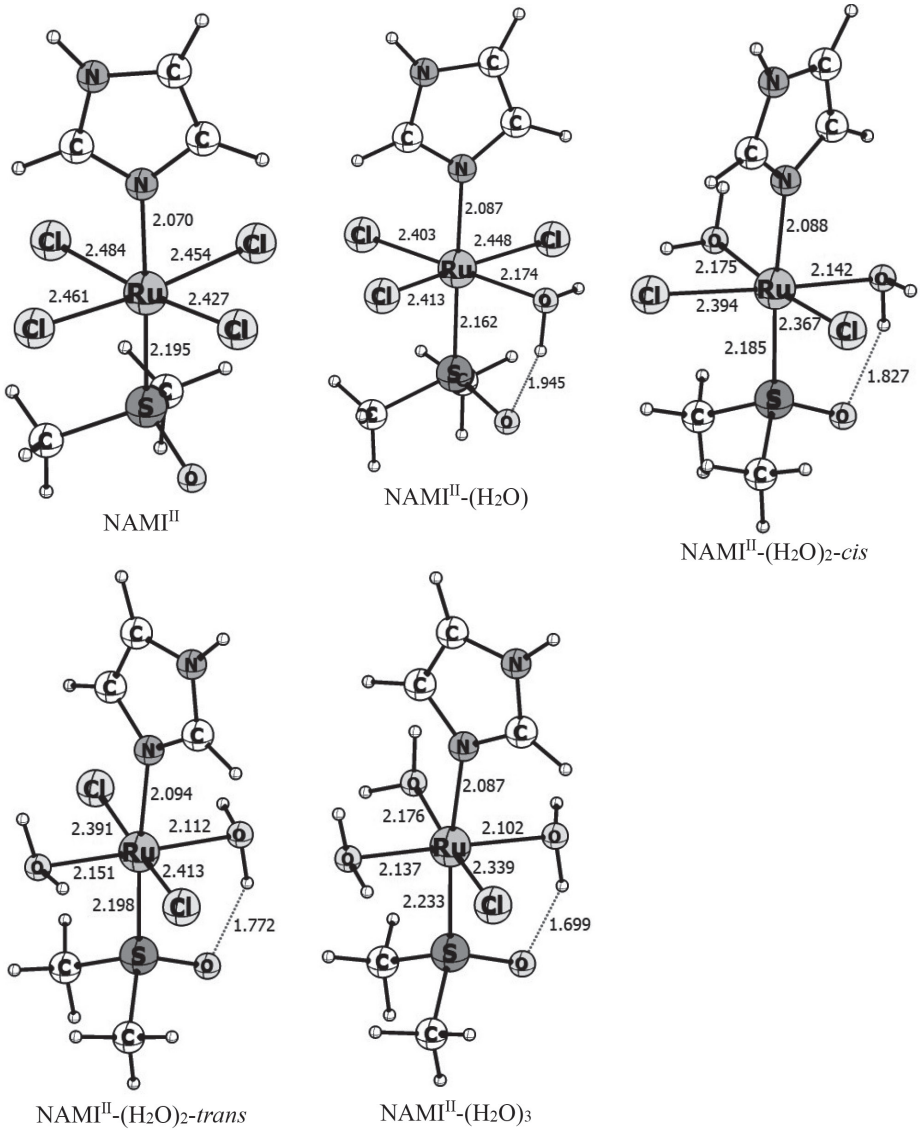

Figure 6. TPSSh/def2-TZVP optimized structures of the reduced form for of NAMI-A complex in the +2 formal oxidation state (NAMI^{II}) and its mono- (NAMI^{II}-(H$_2$O)), di- (NAMI^{II}-(H$_2$O)$_2$-*cis*, NAMI^{II}-(H$_2$O)$_2$-*trans*) and tri- (NAMI^{II}-(H$_2$O)$_3$) water substituted derivatives. Bond distances are given in Å.

was evaluated considering the ruthenium atom in the +3 and +2 formal oxidation states, in order to determine the preferential path for the hydrolysis reaction (pathways a or b, Figure 2). The computed TPSSh/def2-TZVP Gibbs free energies of reaction for the hydrolysis reactions at 298.15 K are quoted in Table 2.

For both NAMI-A and KP1019 in the +2 and +3 oxidation state, the chloride exchange reaction by water is highly favorable and the Gibbs free energy varies almost linearly with the number of water molecules. For instance, as can be seen in Table 2, the free energy for the second and third hydrolysis of NAMI-A is 1.95 and 2.80 times the free energy for the first hydrolysis, respectively, for the +3 oxidation state, and 2.00 and 2.96 for the +2 oxidation state. It is worth noting that the free energy for the first hydrolysis of NAMI-A is almost of the same magnitude for the +2 (–60.4 kcal mol^{-1}) and +3 (–57.4 kcal mol^{-1}) oxidation states, which is also true for the KP1019. However, the hydrolysis with the Ru^{II} is always more favorable than the respective Ru^{III} complexes.

Interestingly, the thermodynamic results reported here correlate well with the Becke, three-parameter, Lee-Yang-Parr (B3LYP)/6-31G(d,p) kinetic data of Vargiu *et al.*,[62] who showed that the activation energy for the first hydrolysis decreases about 3 kcal mol^{-1} with the reduction of NAMI-A. For the second hydrolysis this decrease is even more pronounced, ranging from ca. 7 kcal mol^{-1} for the substitution in *cis* and 9 kcal mol^{-1} for the substitution in *trans* position.[62] These results show that the hydrolysis of the reduced complexes is thermodynamically more favorable and kinetically more accessible than the corresponding Ru^{III} complexes. On the other hand, when

Table 2. Computed Gibbs free energy for the ligand displacement reactions involving water and chloride ligands of NAMI-A and KP1019 complexes in their normal and reduced forms

n	ΔG (for NAMI-A) / (kcal mol^{-1})	
	$[Ru^{III}(Cl)_{4-n}(H_2O)_n(Im)(DMSO)]^{-1+n}$	$[Ru^{II}(Cl)_{4-n}(H_2O)_n(Im)(DMSO)]^{-2+n}$
1	–57.4	–60.4
2	–111.9 (–108.2)[a]	–120.3 (–118.4)[a]
3	–160.4	–178.8
	ΔG (for KP1019) / (kcal mol^{-1})	
	$[Ru^{III}(Cl)_{4-n}(H_2O)_n(Ind)_2]^{-1+n}$	$[Ru^{II}(Cl)_{4-n}(H_2O)_n(Ind)_2]^{-2+n}$
1	–56.5	–53.6
2	–115.1 (–114.0)[a]	–112.7 (–111.4)[a]
3	–175.3	–175.4

[a]Values in parentheses are for the *trans* isomer. NAMI-A: *trans*-tetrachloro(dimethylsulfoxide)imidazole ruthenate(III); Im: imidazole; DMSO: dimethylsulfoxide; KP1019: *trans*-[tetrachlorobis(1*H*-indazole)ruthenate(III)]; Ind: indazole. For the NAMI-A complex the hydrolysis reactions were described as: $[Ru^{III/II}(Cl)_4(Im)(DMSO)]^{-1/-2} + nH_2O \rightarrow [Ru^{III/II}(Cl)_{4-n}(H_2O)_n(Im)(DMSO)]^{-1+n/-2+n} + nCl^-$. For the KP1019 the hydrolysis reactions were described as: $[Ru^{III/II}(Cl)_4(Ind)_2]^{-1/-2} + nH_2O \rightarrow [Ru^{III/II}(Cl)_{4-n}(H_2O)_n(Ind)_2]^{-1+n/-2+n} + nCl^-$. Gibbs free energies were computed at the TPSSh/def2-TZVP/SMD level of theory at 298.15 K.

the same analysis is made for KP1019, we observe that the reduction does not influence the overall Gibbs free energy of the reaction, since the magnitude of the reaction free energy is almost the same for the Ru^{II} and Ru^{III} complexes. This fact may aid in explaining the different mechanism of action of both drugs.

The Gibbs free energy involved in the reduction of NAMI-A and KP1019 is computed as –98.0 and –110.0 kcal mol^{-1}, respectively. Therefore, these results suggest that both complexes have thermodynamic preference to be reduced first, prior to their hydrolysis, thus following pathway b (Figure 2). In fact, solvolysis of the electrochemically generated Ru^{II} species has been observed for both KP1019 and NAMI-A[3,22,23,27] and, in general, the water/chloride exchange reaction is accelerated upon reduction of the Ru^{III} species. However, in the biological medium, it is not straightforward to attribute a preferred pathway for the mechanism of action, since several processes can alter the reduction potential of the drug and, therefore, alter the rate of the solvolysis process. For instance, in the biological medium the prodrugs can be reduced by well-known biological reductants such as reduced nicotinamide adenine dinucleotide (NADH), ascorbate, tocopherol (vitamin E), Cys and GSH, for which the reduction potential at physiological pH is around –0.3 to –0.5 V.[63,64] However, the reaction mechanism involved in the reduction of these complexes is not known and, therefore, in the time scale required for the biological reduction of these prodrugs, solvolysis can takes place. NMR experiments have shown that, under buffered conditions, KP1019 is reduced within 3.5 h in the presence of GSH and within min in the presence of ascorbic acid.[24] It has been suggested that the transport and delivery of the Ru^{III} drugs occur through the interaction with serum proteins such as transferrin and albumin,[17] and ruthenium complexes are not reduced effectively while bound to these proteins.[27] Therefore, aquation can take place prior to reduction and alter the redox properties.

The results reported in Tables 1 and 2 also support the hypothesis that the reduced form of the complexes studied here, as well as their hydrolysis products, are relevant for their antitumor activity, since their formation is thermodynamically favorable and their reduction potentials are biologically accessible. For both complexes, the thermodynamics of the hydrolysis processes are extremely favorable and the Gibbs free energy calculations for the successive hydrolysis reactions revealed that all chloride ligands could be favorably replaced by water. Interestingly, this evidence is in line with the recent work of Keppler and co-workers,[65] who reported the X-ray structure of KP1019 bound to human serum albumin (HSA). The authors showed that KP1019 lost all of the original ligands when crystallized with the protein. An analogous behavior was also observed for the NAMI-A complex and NAMI-A-type complexes.[66,67]

Interactions with biological targets

After being activated, distributed and located in cell compartments, the drug kills the cancer cell through interactions with different cellular components or with DNA. In fact, the primary target for these interactions is still unknown. Wang *et al.*[68] have shown that Ru-based complexes follow different reaction mechanisms than cisplatin in the competitive reaction between S-donor ligands such as

GSH and N-donor ligands. In this mechanism, the reaction between the ruthenium complex and GSH leads to the formation of a ruthenium thiolate compound, which can then undergo oxidation by oxygen to produce an original sulfenate complex. The oxidation of coordinated GSH in the thiolate complex seems to provide an easy route for GSH exchange and Ru-N7 binding formation. This may provide a unique mechanism of action and explain the lack of cross-resistance with platinum drugs, which is a potential clinical advantage. Other cytotoxic activities from NAMI-A and KP1019 may be attributed to their interactions with DNA nucleobases generally to the N7 site of guanine.[17,24] It is worth mentioning that interaction of ruthenium compounds with nucleic acid and derivatives generates compounds with chemical and photophysical properties with important applications in nanotechnologies, medical diagnosis and therapies, and have recently been reviewed by Flamme *et al.*[69]

Since our results suggested that both NAMI-A, KP1019 and their hydrolyzed products are very prone to be reduced, we evaluated the affinity of the NAMI-A and KP1019 for different intracellular components, though the calculation of the thermodynamics of the interaction of the reduced and mono-hydrated forms of NAMI-A and KP1019 with different S-donors (GSH and Cys) and N-donors (GN3 and GN7 sites) ligands.

The TPSSh/def2-TZVP optimized Cartesian coordinates of the free ligands, the protonated form of cysteine and glutathione (CysH and GSH) and guanine, can be found in the SI section. For the GSH, the optimization started with the most stable conformation found at physiological pH, taken from molecular dynamics conformational sampling studies.[70,71] Figure 7 shows the possible adducts that can be formed by the interaction of the mono-aquo species of the reduced forms of NAMI-A ($[Ru(Cl)_3(H_2O)(Im)(DMSO)]^-$, $NAMI^{II}$-H_2O) and KP1019 ($[Ru(Cl)_3(H_2O)(In)_2]^-$, $KP1019^{II}$-H_2O) with the biological molecules. The optimized structures of the adducts are presented in Figures 8 and 9, which highlight the main structural parameters around the metallic center. As can be seen, the complexes exhibit an octahedral arrangement of the ligands, with the angles around the metal deviating from the optimal values for the octahedral geometry.

For each of the reactions showed in Figure 7, we have used a thermodynamic cycle to compute the Gibbs free energy for the ligand displacement reaction in solution, as the one exemplified in Figure 3. The final Gibbs free energy for the interaction in aqueous solution was then computed using equation 3 and the results are quoted in Table 3. As is shown in equation 3, the overall Gibbs free energy of the reaction is composed of two major components: (*i*) the Gibbs free energy of the reaction in

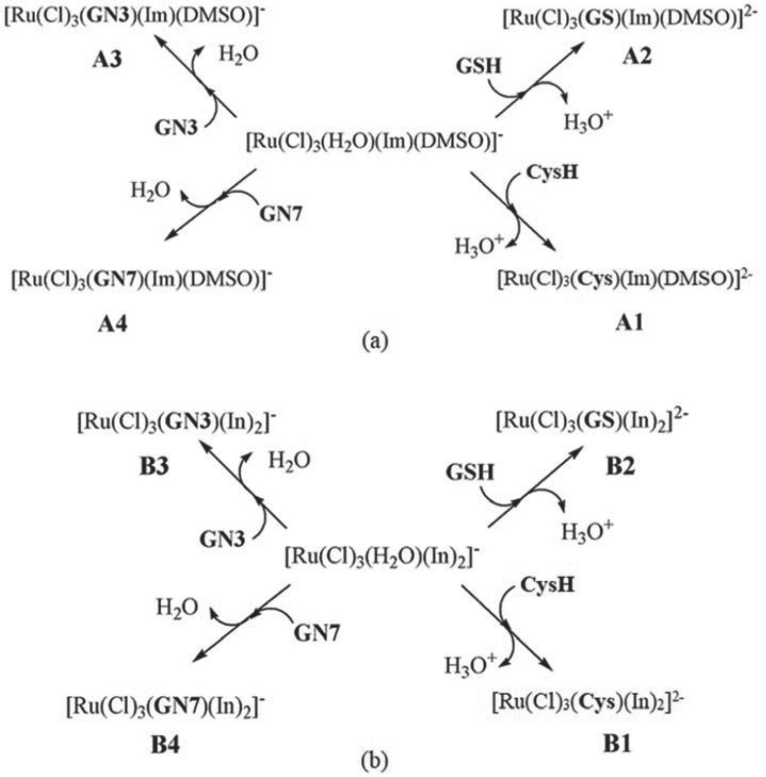

Figure 7. Schematic representation of the reactions between the Ru^{II}-monoaquo complexes of (a) NAMI-A and (b) KP1019 with the GN3 and GN7 sites, CysH and GSH.

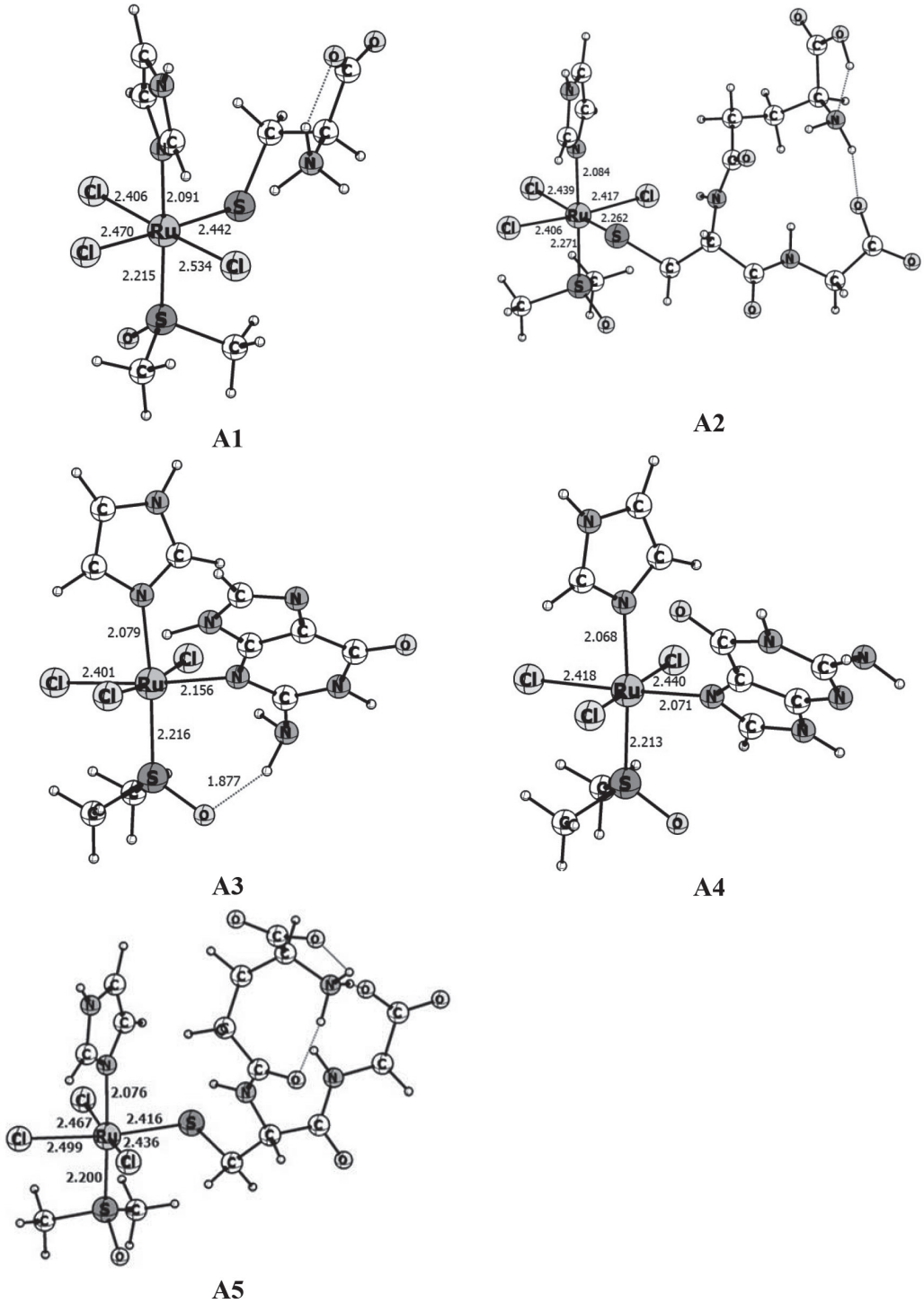

Figure 8. TPSSh/def2-TZVP optimized structures of the adducts formed by the reaction of the mono-aquo species of NAMI-A ($NAMI^{II}$-(H_2O)) with the GN3 and GN7 sites, CysH and GSH. **A1**, **A2**, **A3**, **A4** and **A5** are the structures obtained from the reaction with CysH, GSH in circular conformation, GN3 and GN7 sites and GSH in extended conformation, respectively. Bond distances are given in Å.

gas phase (ΔG_g); and (*ii*) the variation of the solvation free energies of the species.

The results quoted in Table 3 show that the interaction of $NAMI^{II}$-H_2O and $KP1019^{II}$-H_2O complexes with the GN3 site is unfavorable. The interaction with guanine at the GN7 site is only slightly favorable in solution, with ΔG_{sol} = –0.4 kcal mol^{-1} for $NAMI^{II}$-H_2O and –4.8 kcal mol^{-1} for the interaction with $KP1019^{II}$-H_2O. It is interesting to note that the intereaction of both complexes with the depronated form of GSH and Cys, generating the complexes $[RuCl_3(DMSO)(Im)(Cys)]^{2-}$, $[RuCl_3(In)_2(Cys)]^{2-}$, $[RuCl_3(DMSO)(Im)(GS)]^{2-}$,

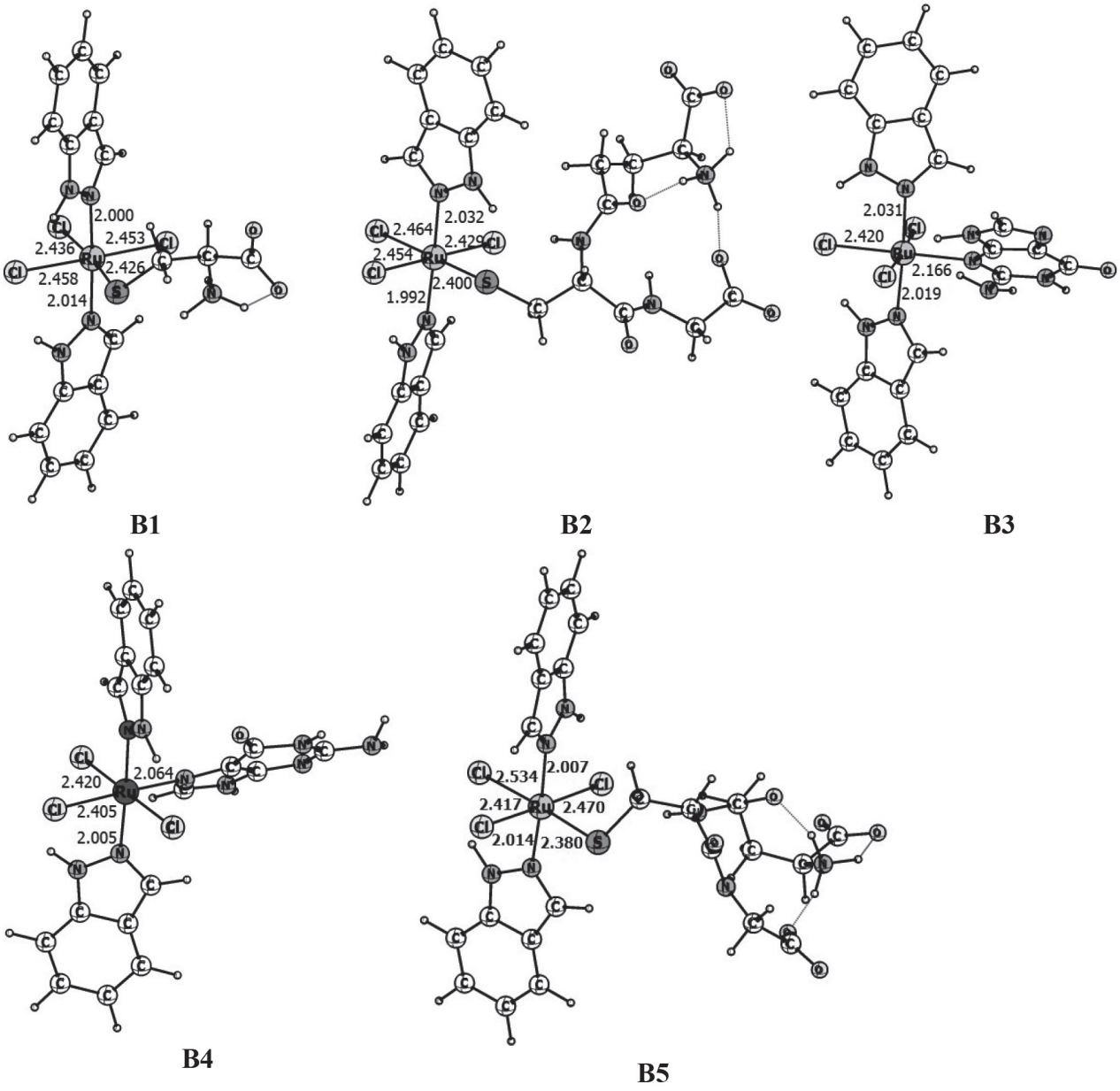

Figure 9. TPSSh/def2-TZVP optimized structures of the adducts formed by the reaction of the mono-aquo species of KP1019 (KP1019^{II}-(H_2O)) with the GN3 and GN7 sites, CysH and GSH. **B1**, **B2**, **B3**, **B4**, **B5** are the structures obtained from the reaction with CysH, GSH in circular conformation, GN3 and GN7 sites and GSH in extended conformation, respectively.

$[RuCl_3(In)_2(GS)]^{2-}$, with overall –2 charge, is highly unfavorable to happen in solution. This may be attributed to the unfavorable interaction between two negatively charged species. On the other hand, the coordination of GSH in the protonated form is slightly favorable for NAMI^{II}-H_2O and KP1019^{II}-H_2O with solvation free energies of –0.7 and –2.6 kcal mol^{-1}, respectively, for the water displacement reaction. Also, displacement of water by the protonated cysteine is also favorable for both complexes. Since it is well known that both NAMI-A and KP1019 interact with GSH under buffered condition,[24] these results suggest, therefore, that the S-donor ligands may interact with the metallodrug in the protonated form, which leads to negative Gibbs free energy of reaction. For both complexes, the interaction with the GN7 site and GSH are of the same magnitude, meaning that these ligands can compete for binding to the metallodrug. And, in the case of KP1019, interaction with Cys is also of the same magnitude. The unfavorable (or only slightly favorable) free energy values for the interaction of the complexes with GN3 and GN7 sites suggest that the principal mechanism of action of NAMI-A and KP1019 may not involve the direct interaction with DNA. Indeed, it has been shown that the cytotoxic activity of KP1019 is

Table 3. Computed Gibbs free energy for the reaction of the Ru^{II}-monoaquo complexes ($NAMI^{II}$-H_2O and $KP1019^{II}$-H_2O) with the GN3 and GN7 sites, CysH and GSH

L	ΔG_{sol} / (kcal mol^{-1})	
	$NAMI^{II}$-H_2O	$KP1019^{II}$-H_2O
GN3	11.3	0.9
GN7	–0.4	–4.8
CysH[a]	20.0 (–11.9)	18.1 (–4.1)
GSH[b]	32.9 [–0.7]	24.6 [–2.6]

[a]Values in parentheses were obtained for the displacement reaction of water by neutral CysH ligand; [b]values in brackets were obtained for the displacement reaction of water by neutral GSH ligand. The reactions involved in the calculations are shown in Figure 7. For each reaction a thermodynamic cycle, as exemplified in Figure 3, was used. ΔG_{sol}: Gibbs free energy for the reaction in solution computed according to equation 3, computed at the TPSSh/def2-TZVP/SMD level of theory at 298.15 K; **L**: biologial target; $NAMI^{II}$-H_2O: $[RuCl_3(DMSO)(Im)(H_2O)]^-$; $KP1019^{II}$-H_2O: $[RuCl_3(In)_2(H_2O)]^-$; GN3 and GN7: guanine nucleobase at the N3 and N7 sites, respectively; CysH: cysteine; GSH: glutathione.

based on ER stress-related effects while NAMI-A interacts with some proteins responsible for DNA replication.[31-35]

Conclusions

In this work, we employed the DFT at the TPSSh/def2-TZVP level, in combination with the SMD continuum solvation model, to investigate the electrochemistry of NAMI-A, KP1019 and their hydrolysis products, as well as the thermodynamics of their interactions with S-donor (CysH and GSH) and N-donor (GN3 and GN7 coordination sites) biological molecules. Our results show that the compounds exhibit different electrochemical behavior upon hydrolysis. The reduction potential of NAMI-A is sensitive to the degree of hydrolysis, increasing with the number of chloride ligands replaced by water. On the other hand, the reduction potential of KP1019 does not vary with the hydrolysis and remains almost constant. Our results showed that thermodynamically, the NAMI-A and KP1019 complexes have a thermodynamic preference to be reduced first and to undergo hydrolysis after, since the free energy involved in the reduction process of the complexes is more negative. For both complexes, the interaction with the GN7 site and GSH are of the same magnitude (ΔG_{sol} ca. –0.6 kcal mol^{-1}) meaning that these ligands can compete for binding to the metallodrug. And, in the case of KP1019, interaction with CysH is also of the same magnitude. The unfavorable (or only slightly favorable) free energy values for the interaction of the complexes with guanine at the N3 and N7 sites suggest that the principal mechanism of action of NAMI-A and KP1019 may not involve the direct interaction with DNA. The calculations showed that the interaction of the complexes with GSH and Cys is only favorable in the neutral or protonated forms, and this is an important information to propose a reaction mechanism for the reduction reaction of these metallodrugs by thiol-like reductants. It is also worth noting that, according to the calculations, once the first hydrolysis takes place the complexes have thermodynamic preference to undergo further hydrolysis than to interact with the S-donor or N-donor ligands studied in this work, and this is somehow in line with recent experimental findings.

As a final note, it is important to mention that, despite the agreements with some experimental evidences, our study was focused on the thermodynamics of the process, to discuss the preferential interactions. However, the kinetics of the processes studied in this work will certainly play an important role in determining the preferential pathway for these competitive interactions.

Supplementary Information

Supplementary information (plot of the frontier molecular orbitals for KP1019, NAMI-A and their hydrolysis products, figures of the optimized structures of the KP1019 complexes and TPSSh/def2-TZVP optimized Cartesian coordinates of all species studied in this work) is available free of charge at http://jbcs.sbq.org.br as PDF file.

Acknowledgments

The authors would like to thank Conselho Nacional de Desenvolvimento Científico e Tecnológico (CNPq; INCT-Catálise) and Fundação de Amparo à Pesquisa do Estado de Minas Gerais (FAPEMIG) for the financial support and research grants.

References

1. Rosenberg, B.; VanCamp, L.; Trosko, J. E.; Mansour, H. V.; *Nature* **1969**, *222*, 385.
2. Rosenberg, B.; Van Camp, L.; Krigas, T.; *Nature* **1965**, *205*, 698.
3. Clarke, M. J.; *Coord. Chem. Rev*. **2003**, *236*, 209.
4. Mjos, K. D.; Orvig, C.; *Chem. Rev*. **2014**, *114*, 4540.
5. Murray, B. S.; Babak, M. V.; Hartinger, C. G.; Dyson, P. J.; *Coord. Chem. Rev*. **2016**, *306*, 86.
6. Johnstone, T. C.; Suntharalingam, K.; Lippard, S. J.; *Chem. Rev.* **2016**, *116*, 3436.
7. Pasini, A.; Zunino, F.; *Angew. Chem., Int. Ed. Engl.* **1987**, *26*, 615.
8. Boulikas, T.; Vougiouka, M.; *Oncol. Rep.* **2003**, *10*, 1663.
9. Smith, N. A.; Sadler, P. J.; *Philos. Trans. R. Soc., A* **2013**, *371*, 20120519.

10. Sava, G.; Pacor, S.; Mestroni, G.; Alessio, E.; *Clin. Exp. Metastasis* **1992**, *10*, 273.
11. Hartinger, C. G.; Jakupec, M. A.; Zorbas-Seifried, S.; Groessl, M.; Egger, A.; Berger, W.; Zorbas, H.; Dyson, P. J.; Keppler, B. K.; *Chem. Biodiversity* **2008**, *5*, 2140.
12. Sava, G.; Bergamo, A.; Zorzet, S.; Gava, B.; Casarsa, C.; Cocchietto, M.; Furlani, A.; Scarcia, V.; Serli, B.; Iengo, E.; Alessio, E.; Mestroni, G.; *Eur. J. Cancer* **2002**, *38*, 427.
13. Leijen, S.; Burgers, S. A.; Baas, P.; Pluim, D.; Tibben, M.; van Werkhoven, E.; Alessio, E.; Sava, G.; Beijnen, J. H.; Schellens, J. H.; *Invest. New Drugs* **2015**, *33*, 201.
14. Sava, G.; Zorzet, S.; Turrin, C.; Francesca, V.; Soranzo, M. R.; Zabucchi, G.; Cocchietto, M.; Bergamo, A.; DiGiovine, S.; Pezzoni, G.; Sartor, L.; Garbisa, S.; *Clin. Cancer Res.* **2003**, *9*, 1898.
15. Gava, B.; Zorzet, S.; Spessotto, P.; Cocchietto, M.; Sava, G.; *J. Pharmacol. Exp. Ther.* **2006**, *317*, 284.
16. Alessio, E.; *Eur. J. Inorg. Chem*. **2017**, *2017*, 1549.
17. Trondl, R.; Heffeter, P.; Kowol, C. R.; Jakupec, M. A.; Berger, W.; Kepler, B. K.; *Chem. Sci*. **2014**, *5*, 2925.
18. Costa, G.; Balducci, G.; Alessio, E.; Tavagnacco, C.; Mestroni, G.; *J. Electroanal. Chem*. **1990**, *296*, 57.
19. Alessio, E.; Balducci, G.; Lutman, A.; Mestroni, G.; Calligaris, M.; Attia, W. M.; *Inorg. Chim. Acta* **1993**, *203*, 205.
20. Hartmann, M.; Lipponer, K.-G.; Kepler, B. K.; *Inorg. Chim. Acta* **1998**, *267*, 137.
21. Frasca, D. R.; Clarke, M. J.; *J. Am. Chem. Soc*. **1999**, *121*, 8523.
22. Ravera, M.; Baracco, S.; Cassino, C.; Zanello, P.; Osella, D.; *Dalton Trans*. **2004**, 2347.
23. Reisner, E.; Arion, V. B.; da Silva, M. F. C. G.; Lichtenecker, R.; Eichinger, A.; Kepler, B. K.; Kukushkin, V. Y.; Pombeiro, A. J. L.; *Inorg. Chem*. **2004**, *43*, 7083.
24. Schluga, P.; Hartinger, C. G.; Egger, A.; Reisner, E.; Galanski, M.; Jakupec, M. A.; Kepler, B. K.; *Dalton Trans*. **2006**, 1796.
25. Ravera, M.; Cassino, C.; Baracco, S.; Osella, D.; *Eur. J. Inorg. Chem*. **2006**, 740.
26. Cebrián-Losantos, B.; Reisner, E.; Kowol, C. R.; Roller, A.; Shova, S.; Arion, V. B.; Kepler, B. K.; *Inorg. Chem*. **2008**, *47*, 6513.
27. Reisner, E.; Arion, V. B.; Kepler, B. K.; Pombeiro, A. J. L.; *Inorg. Chim. Acta* **2008**, *361*, 1569.
28. Lever, A. B. P.; *Inorg. Chem*. **1990**, *29*, 1271.
29. Mestroni, G.; Alessio, E.; Sava, G.; Pacor, S.; Coluccia, M.; Boccarelli, A.; *Met.-Based Drugs* **1994**, *1*, 41.
30. Haukka, M.; Ahlgrén, M.; Pakkanen, T. A.; *J. Chem. Soc., Dalton Trans*. **1996**, 1927.
31. Bergamo, A.; Gaiddon, C.; Schellens, J. H. M.; Beijnen, J. H.; Sava, G.; *J. Inorg. Biochem.* **2012**, *106*, 90.
32. Han Ang, W.; Dyson, P. J.; *Eur. J. Inorg. Chem.* **2006**, *20*, 4003.
33. Qian, C.; Wang, J. Q.; Song, C. L.; Wang, L. L.; Ji, L. N.; Chao, H.; *Metallomics* **2013**, *5*, 844.
34. Bierle, L. A.; Reich, K. L.; Taylor, B. E.; Blatt, E. B.; Middleton, S. M.; Burke, S. D.; Stultz, L. K.; Hanson, P. K.; Partridge, J. F.; Miller, M. E.; *PLoS One* **2015**, *10*, e0138085.
35. Flocke, L. S.; Trondl, R.; Jakupec, M. A.; Keppler, B. K.; *Invest. New Drugs* **2016**, *34*, 261.
36. Smith, C. A.; Sutherland-Smith, A. J.; Kepler, B. K.; Kratz, F.; Baker, E. N.; *J. Biol. Inorg. Chem.* **1996**, *1*, 424.
37. Clarke, M. J.; Zhu, F.; Frasca, D. R.; *Chem. Rev*. **1999**, *99*, 2511.
38. Parr, R. G.; Yang, W.; *Density Functional Theory of Atoms and Molecules*; Oxford University Press: New York, 1989.
39. Staroverov, V. N.; Scuseria, G. E.; Tao, J.; Perdew, J. P.; *J. Chem. Phys*. **2003**, *119*, 12129.
40. Neese, F.; *Wiley Interdiscip. Rev.: Comput. Mol. Sci*. **2012**, *2*, 73.
41. Weigend, F.; Ahlrichs, R.; *Phys. Chem. Chem. Phys*. **2005**, *7*, 3297.
42. van Lenthe, E.; Baerends, E. J.; Snijders, J. G.; *J. Chem. Phys*. **1993**, *99*, 4597.
43. van Lenthe, E.; Baerends, E. J.; Snijders, J. G.; *J. Chem. Phys*. **1994**, *101*, 9783.
44. van Lenthe, E.; van Leeuwen, R.; Baerends, E. J.; Snijders, J. G.; *Int. J. Quantum Chem*. **1996**, *57*, 281.
45. Neese, F.; *J. Comput. Chem*. **2003**, *24*, 1740.
46. Neese, F.; Wennmohs, F.; Hansen, A.; Becker, U.; *Chem. Phys*. **2009**, *356*, 98.
47. Weigend, F.; *Phys. Chem. Chem. Phys*. **2006**, *8*, 1057.
48. Ferreira, D. E. C.; De Almeida, W. B.; Neves, A.; Rocha, W. R.; *Comput. Theor. Chem*. **2012**, *979*, 89.
49. Chagas, M. A.; Rocha, W. R.; *Chem. Phys. Lett*. **2014**, *612*, 78.
50. Chen, J.; Chen, L.; Liao, S.; Zheng, K.; Ji, L.; *Dalton Trans.* **2007**, 3507.
51. Vargiu, A. V.; Robertazzi, A.; Magistrato, A.; Ruggerone, P.; Carloni, P.; *J. Phys. Chem. B* **2008**, *112*, 4401.
52. Rodrigues, G. L. S.; Rocha, W. R.; *J. Phys. Chem. B* **2016**, *120*, 11821.
53. Rulíšek, L.; *J. Phys. Chem. C* **2013**, *117*, 16871.
54. Isse, A. A.; Gennaro, A.; *J. Phys. Chem. B* **2010**, *114*, 7894.
55. Marenich, A. V.; Cramer, C. J.; Truhlar, D. G.; *J. Phys. Chem. B* **2009**, *113*, 6378.
56. Klamt, A.; Schuurmann, G.; *J. Chem. Soc., Perkin Trans. 2* **1993**, 799.
57. Peti, W.; Pieper, T.; Sommer, M.; Keppler, B. K.; Giester, G.; *Eur. J. Inorg. Chem*. **1999**, *1999*, 1551.
58. Brindell, M.; Piotrowska, D.; Shoukry, A. A.; Stochel, G.; van Eldik, R.; *J. Biol. Inorg. Chem.* **2007**, *12*, 809.
59. Brindell, M.; Stawoska, I.; Supel, J.; Skoczowski, A.; Stochel, G.; van Eldik, R.; *J. Biol. Inorg. Chem.* **2008**, *13*, 909.
60. Srnec, M.; Chalupsky, J.; Fojta, M.; Zendlova , L.; Havran, L.; Hocek, M.; Kyvala, M.; Rulíšek, L.; *J. Am. Chem. Soc*. **2008**, *130*, 10947.

61. Rulíšek, L.; *J. Phys. Chem. C* **2013**, *117*, 16871.
62. Vargiu, A. V.; Robertazzi, A.; Magistrato, A.; Ruggerone, P.; Carloni, P.; *J. Phys. Chem. B* **2008**, *112*, 4401.
63. Hamer, M.; Suarez, S. A.; Neuman, N. I.; Alvarez, L.; Muñoz, M.; Marti, M. A.; *Inorg. Chem*. **2015**, *54*, 9342.
64. Suarez, A. A.; Neuman, N. I.; Muñoz, M.; Álvarez, L.; Bikiel, D. E.; Brondino, C. D.; Ivanović-Burmazović, I.; Miljkovic, J. L.; Filipovic, M. R.; Martí, M. A.; Doctorovich, F.; *J. Am. Chem. Soc*. **2015**, *137*, 4720.
65. Bijelic, A.; Theiner, S.; Keppler, B. K.; Rompel, A.; *J. Med. Chem*. **2016**, *59*, 5894.
66. Levina, A.; Lay, P. A.; *Inorg. Chem. Front.* **2014**, *1*, 44.
67. Casini, A.; Temperini, C.; Gabbiani, C.; Supuran, C. T.; Messori, L.; *ChemMedChem* **2010**, *5*, 1989.
68. Wang, F.; Xu, J.; Wu, K.; Weidt, S. K.; Mackay, C. L.; Langridge-Smith, P. R. R.; Sadler, P. J.; *Dalton Trans.* **2013**, *42*, 3188.
69. Flamme, M.; Clarke, E.; Gasser, G.; Hollenstein, M.; *Molecules* **2018**, *23*, 1515.
70. Lampela, O.; Juffer, A. H.; Rauk, A.; *J. Phys. Chem. A* **2003**, *107*, 9208.
71. Zhang, R.; Wu, W.; Luo, S.; *J. Solution Chem*. **2011**, *40*, 1784.

Submitted: August 5, 2018
Published online: October 11, 2018